

RESEARCH ARTICLE

Open Access

Claudin-low-like mouse mammary tumors show distinct transcriptomic patterns uncoupled from genomic drivers



Christian Fougner¹, Helga Bergholtz¹, Raoul Kuiper², Jens Henrik Norum¹ and Therese Sørlie^{1,3,4*} 

Abstract

Background: Claudin-low breast cancer is a molecular subtype associated with poor prognosis and without targeted treatment options. The claudin-low subtype is defined by certain biological characteristics, some of which may be clinically actionable, such as high immunogenicity. In mice, the medroxyprogesterone acetate (MPA) and 7, 12-dimethylbenzanthracene (DMBA)-induced mammary tumor model yields a heterogeneous set of tumors, a subset of which display claudin-low features. Neither the genomic characteristics of MPA/DMBA-induced claudin-low tumors nor those of human claudin-low breast tumors have been thoroughly explored.

Methods: The transcriptomic characteristics and subtypes of MPA/DMBA-induced mouse mammary tumors were determined using gene expression microarrays. Somatic mutations and copy number aberrations in MPA/DMBA-induced tumors were identified from whole exome sequencing data. A publicly available dataset was queried to explore the genomic characteristics of human claudin-low breast cancer and to validate findings in the murine tumors.

Results: Half of MPA/DMBA-induced tumors showed a claudin-low-like subtype. All tumors carried mutations in known driver genes. While the specific genes carrying mutations varied between tumors, there was a consistent mutational signature with an overweight of T>A transversions in TG dinucleotides. Most tumors carried copy number aberrations with a potential oncogenic driver effect. Overall, several genomic events were observed recurrently; however, none accurately delineated claudin-low-like tumors. Human claudin-low breast cancers carried a distinct set of genomic characteristics, in particular a relatively low burden of mutations and copy number aberrations. The gene expression characteristics of claudin-low-like MPA/DMBA-induced tumors accurately reflected those of human claudin-low tumors, including epithelial-mesenchymal transition phenotype, high level of immune activation, and low degree of differentiation. There was an elevated expression of the immunosuppressive genes *PTGS2* (encoding COX-2) and *CD274* (encoding PD-L1) in human and murine claudin-low tumors.

Conclusions: Our findings show that the claudin-low breast cancer subtype is not demarcated by specific genomic aberrations, but carries potentially targetable characteristics warranting further research.

Keywords: Breast cancer, Claudin-low, Subtypes, Genomics, Transcriptomics, Mouse models, DMBA, MPA

* Correspondence: therese.sorlie@rr-research.no

¹Department of Cancer Genetics, Oslo University Hospital, Oslo, Norway

³Centre for Cancer Biomarkers CCBIO, University of Bergen, Bergen, Norway

Full list of author information is available at the end of the article



Background

The claudin-low subtype of breast cancer (BC) is a distinct disease entity associated with a relatively poor prognosis, and with an inadequately understood clinical significance [1–3]. It is characterized by low expression of tight junction and cell-cell adhesion genes, low degree of differentiation, epithelial-mesenchymal transition (EMT) phenotype, and high level of immune cell infiltration [2]. The claudin-low subtype represents 7–14% of all breast cancers, and despite its unique biological features, there are no therapies specifically targeting the subtype [2–5]. While claudin-low tumors are found in several large-scale studies, there is a paucity of information regarding their specific genomic characteristics [6–9]. Thus, significant gaps remain in the understanding of the biology of claudin-low tumors, and there is a need for further research to explore how their unique features may be therapeutically targeted.

Accurate preclinical models are vital for research into novel treatment options. Mouse mammary tumors may be induced through exposure to medroxyprogesterone acetate (MPA) and 7,12-dimethylbenzanthracene (DMBA) [10]. The tumors generated by this protocol are diverse, and a subset of these show similarities to the human claudin-low subtype [11, 12]. A homogeneous primary in vivo model of claudin-low breast cancer does not currently exist [11]. While the mechanisms of MPA [10, 13] and DMBA [14–17] have been described, there is still contention regarding the suitability of a chemically induced model of cancer for a disease that is not primarily caused by carcinogens in humans [18]. Evaluating the claudin-low subset of MPA/DMBA-induced tumors as a model for human disease is therefore an important step toward advancing preclinical research of claudin-low breast cancer.

In this study, we identified and comprehensively characterized claudin-low-like mouse mammary tumors generated by MPA/DMBA-induced carcinogenesis. Through genomic and transcriptomic analyses, we evaluated these tumors as a model for human claudin-low breast cancer and showed these tumors to be phenotypically accurate representations of their human counterparts. In parallel, we analyzed the previously unexplored genomic features of human claudin-low breast cancer. Our findings highlighted several features of claudin-low breast cancer with potential therapeutic implications, including a low tumor mutational burden, high expression of the immune checkpoint gene *CD274* (encoding PD-L1), and high expression of *PTGS2* (encoding cyclooxygenase-2).

Methods

Mouse strains and tumor induction

Double transgenic mice, *Lgr5-EGFP-Ires-CreERT2;R26R-Confetti* [19], were generated by crossing heterozygous *Lgr5-EGFP-Ires-CreERT2* mice with heterozygous *R26R-*

Confetti mice. These transgenes are considered biologically inert and all female offspring, including wild type, single, or double transgenic mice, were used for MPA/DMBA-treatment experiments. All mice were locally bred and maintained within a specific pathogen-free barrier facility according to local and national regulations, with food and water ad libitum. Female mice were treated with medroxyprogesterone acetate (MPA) and 7,12-dimethylbenzanthracene (DMBA) in accordance with the established protocol [10]. In brief, 90-day release MPA pellets (50 mg/pellet, Innovative Research of America cat.# NP-161) were implanted subcutaneously at 6 and 19 weeks after birth. One microgram of DMBA (Sigma Aldrich cat.# D3254) dissolved in corn oil (Sigma Aldrich cat.# C8267) was administered by oral gavage at 9, 10, 12, and 13 weeks after birth. Tumor growth was regularly monitored by manual palpation and measured by a caliper. Tumor volume was estimated using the following formula: volume = (width² × length)/2. When the tumors reached the maximum allowed size of 1000 mm³, or at the age of 32 weeks, tissue was collected at necropsy and fixed in 4% paraformaldehyde (PFA) or snap frozen and stored at –80 °C. Eighteen tumors from 14 mice, of which four mice carried two mammary tumors, were subject to genomic and transcriptomic analyses. Six normal mammary glands collected from mice not undergoing MPA/DMBA treatment were included as controls. Mouse features and histopathological tumor features can be found in Additional file 1.

Histopathology and immunohistochemistry

Mouse tissue was fixed overnight in 4% PFA, routinely processed and paraffin embedded. Formalin-fixed paraffin-embedded tissue was sectioned and stained with hematoxylin and eosin (HE). HE-stained tissue was classified by a certified veterinary pathologist. Immunohistochemical staining was performed as previously described [20] with primary antibodies against K5 (Covance cat.# PRB-160P), K18 (Progen cat.# 61028), Ki67 (Novocastra cat.# NCL-Ki67p), ER α (Millipore cat.# 06-935), PR (Abcam cat.# ab131486), and Her2/Erbb2 (Millipore cat.# 06-562).

DNA and RNA isolation

DNA isolation for exome sequencing was carried out at Theragen Etx Bio Institute (Seoul, South Korea). DNA was isolated using QIAamp DNA Mini Kit (Qiagen cat.# 51306) per the manufacturer's protocol. DNA from two samples (*S159_14_11* and *S176_14_11*) was isolated using CTAB Extraction Solution (Biosesang cat.# C2007) per the manufacturer's protocol. DNA integrity was assessed by electrophoresis, and concentration was determined using the Nanodrop ND-1000 spectrophotometer (Thermo Scientific cat.# ND-1000) and Qubit fluorometer (Thermo Scientific cat.# Q33226). Total RNA and DNA

isolation for gene expression microarrays was carried out using the QIAcube system (Qiagen cat.# 9001292) with the AllPrep DNA/RNA Universal Kit (Qiagen cat.# 80224) according to the protocol provided by the supplier, with 30-mg tissue as input. The tissue was manually minced with a scalpel on ice followed by lysis and homogenization using TissueLyzer LT (Qiagen cat.# 85600) and Qias shredder (Qiagen cat.# 79654), respectively. Nucleic acid concentrations were measured by NanoDrop ND-1000 spectrophotometer, and RNA integrity was analyzed using Agilent 2100 Bioanalyzer (Agilent Technologies cat.# G2939BA).

Gene expression microarrays

Gene expression profiling was performed using RNA isolated from 18 snap-frozen MPA/DMBA-induced tumors and six normal/untreated mouse mammary gland samples. Whole genome expression data was obtained using Agilent SurePrint G3 Mouse Gene Expression 8x60K microarrays (Agilent Technologies cat.# G4852B) with Low Input Quick Amp Labeling protocol (Agilent Technologies cat.# 5190-2331) and the Cy3 fluorophore. Forty nanogram RNA was used for input. Microarrays were scanned using an Agilent SureScan Microarray Scanner (Agilent Technologies cat.# G4900DA), and data was extracted using Agilent Feature Extraction software. One tumor sample (*S422_15_2*) failed quality control and was excluded from further gene expression analyses.

Gene expression analyses

Gene expression data was analyzed using Qlucore Omics Explorer 3.2 (Qlucore AB) and R version 3.3.2 [21]. Gene expression values were quantile normalized, and probes with a standard deviation of less than 2.8% of the largest observed standard deviation were filtered out. For genes represented by more than one probe, mean expression values were calculated to obtain one gene expression value per gene. Principal component analysis was performed to assess data quality, and one normal mammary gland sample (*S178_14_2*) was identified as an outlier and removed from further analysis. Murine subtypes were determined by first calculating centroids for each subtype using the original data from Pfefferle et al. [11], followed by calculating Spearman correlation for every sample to each of the subtype centroids. The subtype with the highest correlation coefficient was assigned as the sample's subtype. Two tumor clusters were identified by hierarchical clustering using the murine intrinsic gene list [11], and SigClust [22] was used to test the significance of the difference between the clusters.

Unsupervised hierarchical clustering was performed using average linkage and Spearman correlation as the distance metric. Immune cell infiltration was inferred using ESTIMATE [23]. Scores for gene signatures relevant to

the claudin-low subtype (adhesion, EMT, luminalness, proliferation, vascular content, immunosuppression, and interferons [2, 24–27]) were calculated using a standard (Z) score approach: for every gene in each signature, a standardized expression value was calculated by subtracting the mean across all samples, then dividing by the standard deviation. Calculation of the mean of the standardized expression values across all genes in the signature yielded the score. Gene lists included in the different signatures are found in Additional file 2. The degree of differentiation was calculated using a differentiation predictor [2]. Two-tailed Wilcoxon rank-sum tests were used for statistical testing of differences in scores between two groups.

Whole exome sequencing

Whole exome sequencing was carried out at Theragen Etx Bio Institute. Library preparation and target enrichment was carried out using the SureSelect XT Mouse All Exon Kit (Agilent cat.# 5190-4641) per the manufacturer's instructions. Sequencing was performed on an Illumina HiSeq 2500 (Illumina cat.# SY-401-2501). DNA was sequenced to an average depth of 58. Quality control was performed with FastQC [28].

Sequence alignment and processing

Adapter sequences were removed using CutAdapt, version 1.10 [29]. Low-quality reads were trimmed using Sickle version 1.33 [30], in paired end mode with quality threshold set to 20 and length threshold set to 50 base pairs. Reads were aligned to the mm10 reference genome using the Burrows-Wheeler MEM aligner (BWA-MEM), version 0.7.12 [31]. Following alignment, duplicate reads were marked using Picard (<https://broadinstitute.github.io/picard/>) version 2.0.1. Base quality scores were then recalibrated using GATK version 3.6.0 [32–34]. Lists of known single nucleotide polymorphisms and indels for the FVB/N mouse strain were downloaded from the Mouse Genomes Project, dbSNP release 142, and used for base quality score recalibration and mutation filtering [35].

Mutation calling and analysis

Somatic mutations were called using the MuTect2 algorithm in GATK [32–34] with a minimum allowed base quality score of 20. Mutations were filtered against variants found in matched normal liver tissue and known single nucleotide polymorphisms for the FVB/N mouse strain. Candidate somatic mutations which did not pass the standard MuTect2 filters were removed from further analysis. Mutations not meeting the following requirements were also removed from further analysis: minimum allele depth of 10, minimum allele frequency of 0.05, and presence of the mutation in both forward and reverse strands. Mutations were annotated using SnpEff

[36] and filtered for downstream analysis using SnpSift [37]. Candidate driver mutations were defined as moderate or high impact mutations, as defined by SnpEff, in driver genes as identified by the COSMIC cancer gene census [38]. To identify hotspot mutations, mouse amino acid positions were aligned to the orthologous human amino acid position using Clustal Omega [39] through UniProtKB [40] and used to query mutations found in the COSMIC database [38]. Mutational spectrum and signature analysis was performed using the deconstructSigs framework [41] modified to allow the use of the mm10 mouse reference genome. The COSMIC mutational signatures were used for reference [42].

Copy number aberration analyses

Copy number aberrations were identified from exome sequence data using EXCAVATOR2 [43] using the mm10 reference genome. CNA calling was performed using standard settings and a window size of 20000 bp. Potential driver CNAs were identified by filtering for CNAs associated with cancer in the COSMIC cancer gene census [38].

Analyses of human breast cancer data

Processed data from the METABRIC [6, 7] and TCGA [44] cohorts were downloaded from or analyzed directly on the cBioportal platform [45, 46].

Plot generation

Plots were created using R version 3.3.2 [21]. Heatmaps were created using ComplexHeatmap [47]. Mutational spectrum histograms were created using the deconstructSigs package [41]. All other plots were generated using the ggplot2 package [48].

Results

Gene expression subtyping reveals two distinct tumor clusters

We determined the murine transcriptomic subtypes of 17 MPA/DMBA-induced mammary tumors from 13 mice (Additional file 1) by calculating each tumor's Spearman correlation to the murine subtype centroids [11]. This revealed nine murine subtypes in the cohort (Table 1, Additional file 3), which separated into two distinct clusters upon hierarchical clustering (Fig. 1, $p = 0.044$, SigClust [22]). One cluster consisted of claudin-low^{Ex} and squamous-like^{Ex} tumors, both of which have been shown to resemble the human claudin-low subtype [11]; this is therefore referred to as the claudin-low-like cluster. The other cluster contained tumors from seven different subtypes and is referred to as the mixed cluster. In four instances, two tumors from different mammary glands were harvested from the same mouse. These were classified as

Table 1 Subtype distribution of MPA/DMBA-induced tumors and normal mouse mammary gland tissue

No. of samples	Murine subtype	Cluster
6	Claudin-low ^{Ex}	Claudin-low-like
2	Squamous-like ^{Ex}	Claudin-low-like
3	PyMT ^{Ex}	Mixed
1	Class3 ^{Ex}	Mixed
1	Class8 ^{Ex}	Mixed
1	Class14 ^{Ex}	Mixed
1	ErbB2-like ^{Ex}	Mixed
1	Wnt1-Early ^{Ex}	Mixed
1	Wnt1-Late ^{Ex}	Mixed
5 (normal mammary)	Normal ^{Ex}	Normal

different subtypes in all cases and are presumed to be distinct primary tumors. All normal mammary gland samples were classified as normal-like^{Ex} and clustered separately from the tumors.

Histopathological analysis corroborated the intertumor heterogeneity that was demonstrated by subtyping (Additional file 1). Five of the eight claudin-low-like tumors, including both squamous-like^{Ex} tumors, showed a squamous appearance, while no tumors in the mixed cluster displayed this histological phenotype ($p = 0.009$, Fisher's exact test). There was also a higher frequency of claudin-low-like tumors showing marked neutrophil infiltration ($p = 0.002$, Fisher's exact test) and displaying a marked or partial spindle appearance ($p = 0.050$, Fisher's exact test) compared to tumors in the mixed cluster.

Mutations in MPA/DMBA-induced mammary tumors are independent of gene expression subtype

To determine the genetic characteristics of the tumors, we performed exome sequencing to a mean depth of 58, with 84% of bases being sequenced to a coverage of 20× or higher. We identified a mean of 589 mutations per tumor (range 288 to 1795), corresponding to a mean mutation rate of 11.9 mutations per megabase (range 5.8 to 36.2) (Fig. 2a). This was substantially higher than the average 1.3 mutations per megabase found in human breast cancer [49]. The mutational rate in MPA/DMBA-induced mammary tumors was also relatively high when compared to other chemically induced murine tumors (range 1.4 to 13.0 mutations per megabase) [50–52] and when compared to tumors arising in genetically engineered mouse models (range 0.1 to 0.7 mutations per megabase) [52–57]. There was no significant difference in mutational burden between the tumors in the claudin-low-like and the mixed cluster, and the only subtype-specific trend was a particularly high mutational burden in the two squamous-like^{Ex} tumors (Fig. 2a).

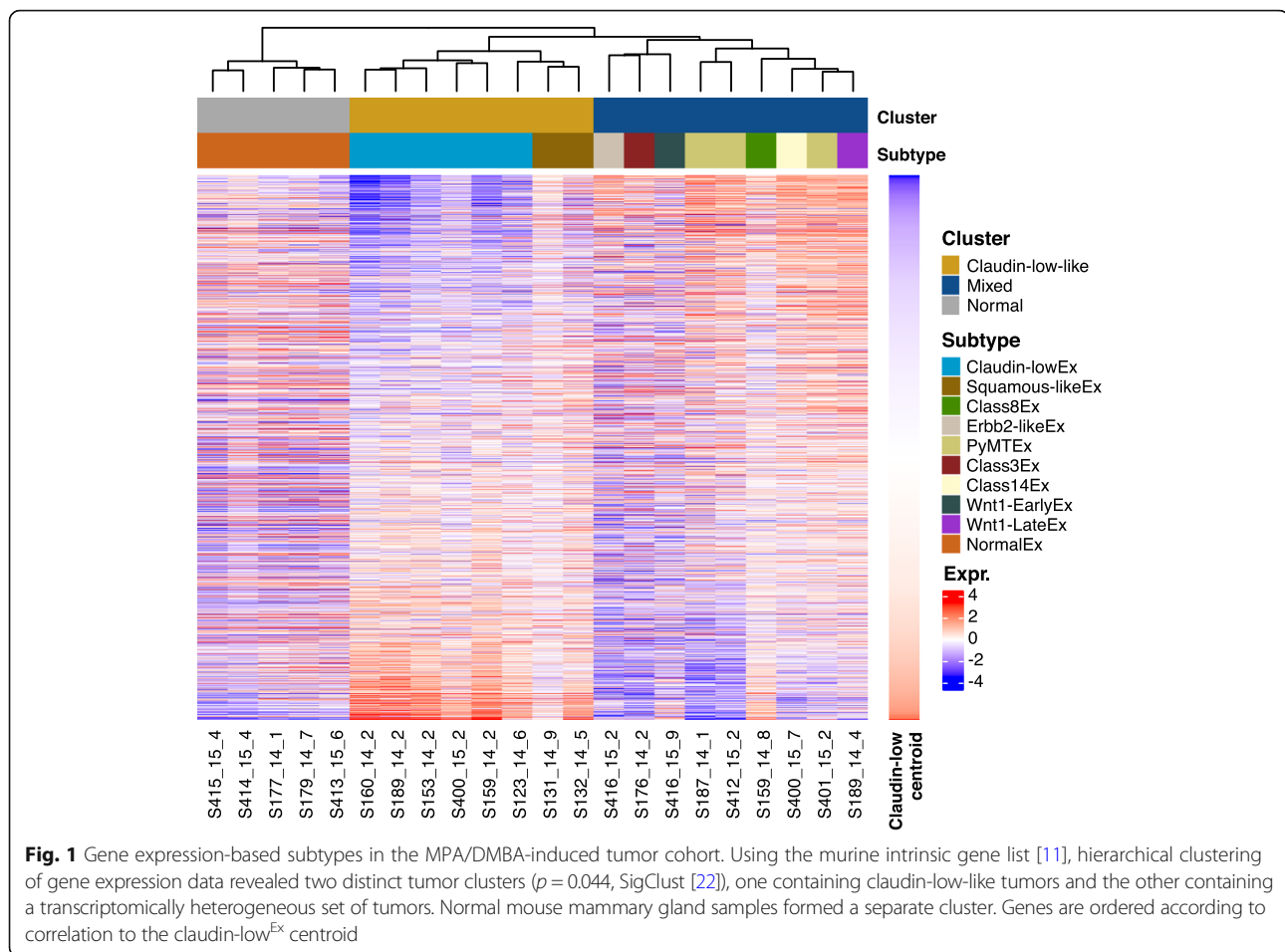


Fig. 1 Gene expression-based subtypes in the MPA/DMBA-induced tumor cohort. Using the murine intrinsic gene list [11], hierarchical clustering of gene expression data revealed two distinct tumor clusters ($p = 0.044$, SigClust [22]), one containing claudin-low-like tumors and the other containing a transcriptomically heterogeneous set of tumors. Normal mouse mammary gland samples formed a separate cluster. Genes are ordered according to correlation to the claudin-low^{Ex} centroid

All tumors carried mutations in driver genes defined by the COSMIC cancer gene census [38], with a mean of 13.8 driver genes carrying mutations per tumor (range 4 to 29) (Fig. 2b). Several driver genes were recurrently mutated, including *Trp53*, *Kras*, and *Kmt2c* (Additional file 4), but no driver genes carried mutations at a significantly different rate between the two clusters. We did, however, identify two notable trends which did not reach statistical significance: an elevated rate of *Trp53* mutations in the claudin-low-like cluster (50% vs. 11%, $p = 0.13$, two-tailed Fisher's exact test) and an elevated rate of *Zfx3* mutations also in the claudin-low-like cluster (37.5% vs. 0%, $p = 0.08$, two-tailed Fisher's exact test). No mutations were significantly associated with histological features.

MPA/DMBA-induced tumors and human breast cancers display disparate gene mutational profiles

To narrow down potential driver mutations in the MPA/DMBA-induced tumors, we compared amino acid changes caused by mutations in driver genes to known amino acid changes in human cancers [38] (Table 2, Additional file 5). There were hotspot amino acid

changes in all *Ras* genes, including *Kras* G12C, G13R, Q61H, *Hras* Q61L, and *Nras* Q61L. In total, 8 of 18 tumors carried hotspot amino acid changes in *Ras* genes. There was one *Pik3ca* mutation in the cohort causing an H1047R amino acid change. This mutation is frequently found in human breast cancer and has previously been reported in DMBA-induced mouse mammary tumors [58].

There were marked disparities between the gene mutational profiles of human breast cancer [44] and MPA/DMBA-induced tumors (Fig. 2c, Additional file 6). The two most frequently mutated genes in breast cancer are *PIK3CA* and *TP53*. While *TP53* showed comparable mutation rates between human breast cancer and MPA/DMBA-induced tumors (34% and 28%, respectively), *PIK3CA* mutation does not appear to be a common event in MPA/DMBA-induced tumors (35% in BC, 6% in MPA/DMBA). Several frequently mutated genes in breast cancer, such as *CDHI*, *GATA3*, and *MAP3K1*, were not mutated in any MPA/DMBA-induced tumors. Conversely, many genes frequently mutated in MPA/DMBA-induced tumors, such as *ATR*, *FAT1*, and *KRAS*, are rarely mutated in breast cancer.

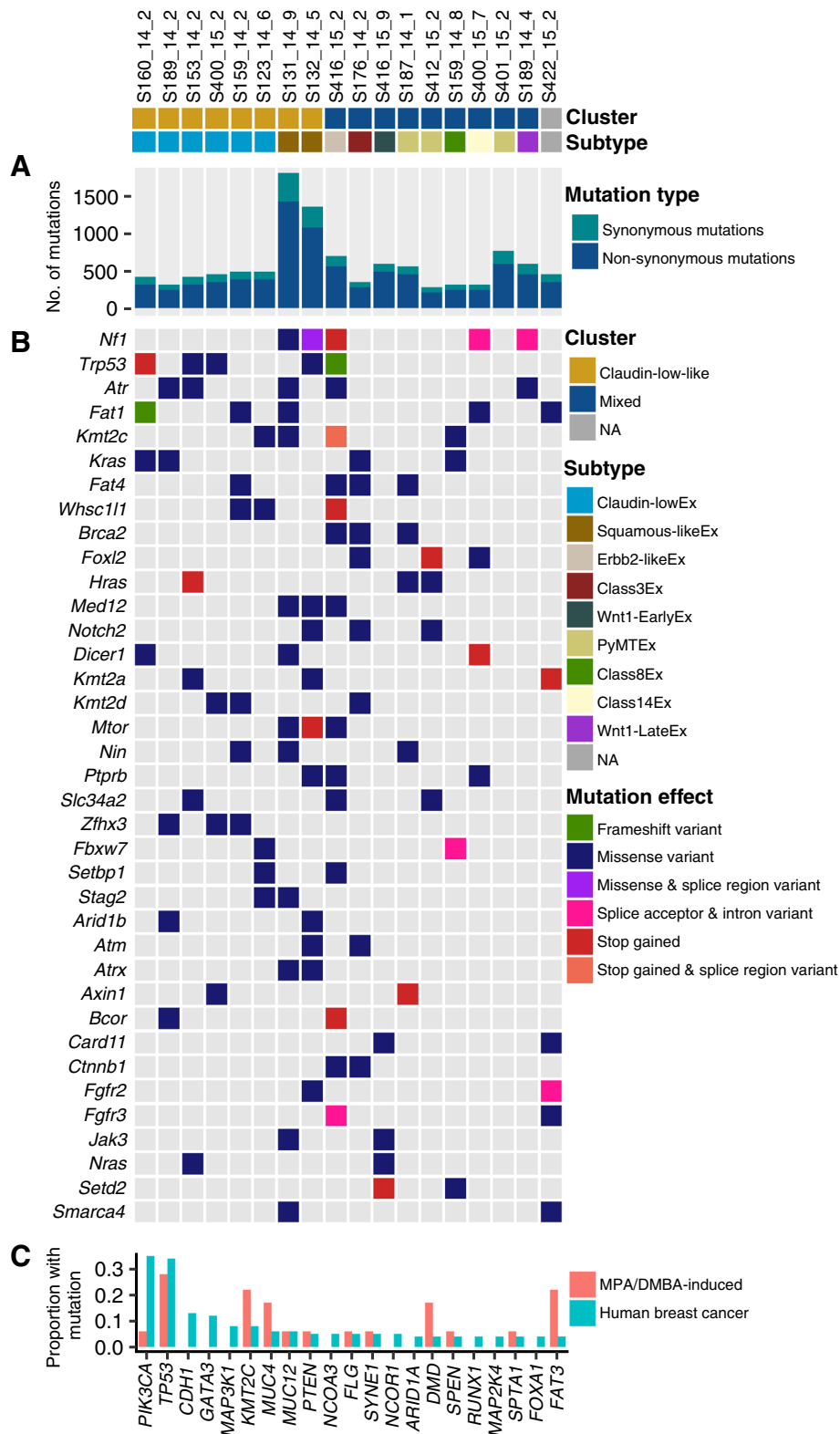


Fig. 2 (See legend on next page.)

(See figure on previous page.)

Fig. 2 Somatic mutations in MPA/DMBA-induced mouse mammary tumors. **a** The MPA/DMBA-induced tumors carried between 288 and 1795 exonic mutations. No significant differences in mutational burden were found between the clusters; however, a high mutational rate was observed in the two squamous-like^{Ex} tumors. **b** *Nf1*, *Trp53*, *Atr*, and *Fat1* were the most frequently mutated driver genes in the MPA/DMBA-induced tumor cohort. No specific mutations accurately delineated the tumor clusters. **c** MPA/DMBA-induced tumors generally showed divergent mutational rates compared to human breast cancer in the genes most frequently mutated in human breast cancer. *TP53* mutations occurred at a similar rate in MPA/DMBA-induced tumors and human breast cancer

DMBA induces a characteristic mutational spectrum with a high frequency of T>A transversions in TG dinucleotides

To characterize the mutagenic profile of DMBA, we analyzed the mutational spectra of the MPA/DMBA-induced tumors. Mutations showed a majority of T>A transversions, which accounted for 63% of all mutations (Additional file 7A). In their trinucleotide context, thymine mutations (T>N) were overrepresented in positions with a 3' guanine nucleotide (Additional file 7B and C, Additional file 8). This was statistically significant when compared to the proportion of thymine nucleotides in an NTG context in the mouse reference genome ($p < 0.001$ in all cases, two-tailed Wilcoxon rank-sum test). There was a similar overrepresentation of cytosine mutations in positions with a 3' adenine. This was statistically significant for C>A and C>G mutations ($p < 0.001$), but not for C>T mutations ($p = 0.089$), when compared to the proportion of cytosine nucleotides in an NCA context in the mouse reference genome.

Mutation signature analysis revealed evidence of signatures 4, 6, 22, 24, and 25 [42] in the MPA/DMBA-induced tumors (Additional file 7D). All tumors were associated with signature 22, while signatures 4 and 25 were found in 17 and 11 of the 18 tumors, respectively.

Table 2 Selected hotspot mutations in MPA/DMBA-induced tumors

Sample	Gene	Amino acid change
S176_14_2	<i>Ctnnb1</i>	Asp32Asn
S416_15_2	<i>Ctnnb1</i>	Thr41Ile
S187_14_1	<i>Hras</i>	Gln61Leu
S412_15_2	<i>Hras</i>	Gln61Leu
S159_14_8	<i>Kras</i>	Gly12Cys
S160_14_2	<i>Kras</i>	Gly12Cys
S176_14_2	<i>Kras</i>	Gly13Arg
S189_14_2	<i>Kras</i>	Gln61His
S153_14_2	<i>Nras</i>	Gln61Leu
S416_15_9	<i>Nras</i>	Gln61Leu
S187_14_1	<i>Pik3ca</i>	His1047Arg
S132_14_5	<i>Trp53</i>	His211Pro
S153_14_2	<i>Trp53</i>	Lys129Met
S400_15_2	<i>Trp53</i>	Gln141Pro
S400_15_2	<i>Trp53</i>	His211Pro

Signatures 24 and 6 were only found in four and one tumor(s), respectively. Notably, none of the signatures found in MPA/DMBA-induced tumors have been associated with human breast cancer [42].

MPA/DMBA-induced tumors have diverse copy number profiles

Breast cancer is largely driven by copy number aberrations (CNAs) [59], yet the copy number profiles of MPA/DMBA-induced mammary tumors have not previously been described. We found a mean of 1299 genes with CNA per tumor (range 90–3057), of which a mean of 65% were amplifications. There was a tendency for claudin-low-like tumors to have a lower burden of CNAs, with a mean of 919 genes carrying CNA, compared to the mixed group of tumors, with a mean of 1637 genes carrying CNA (Fig. 3a). This trend did however not reach statistical significance ($p = 0.139$, two-tailed Wilcoxon rank-sum test).

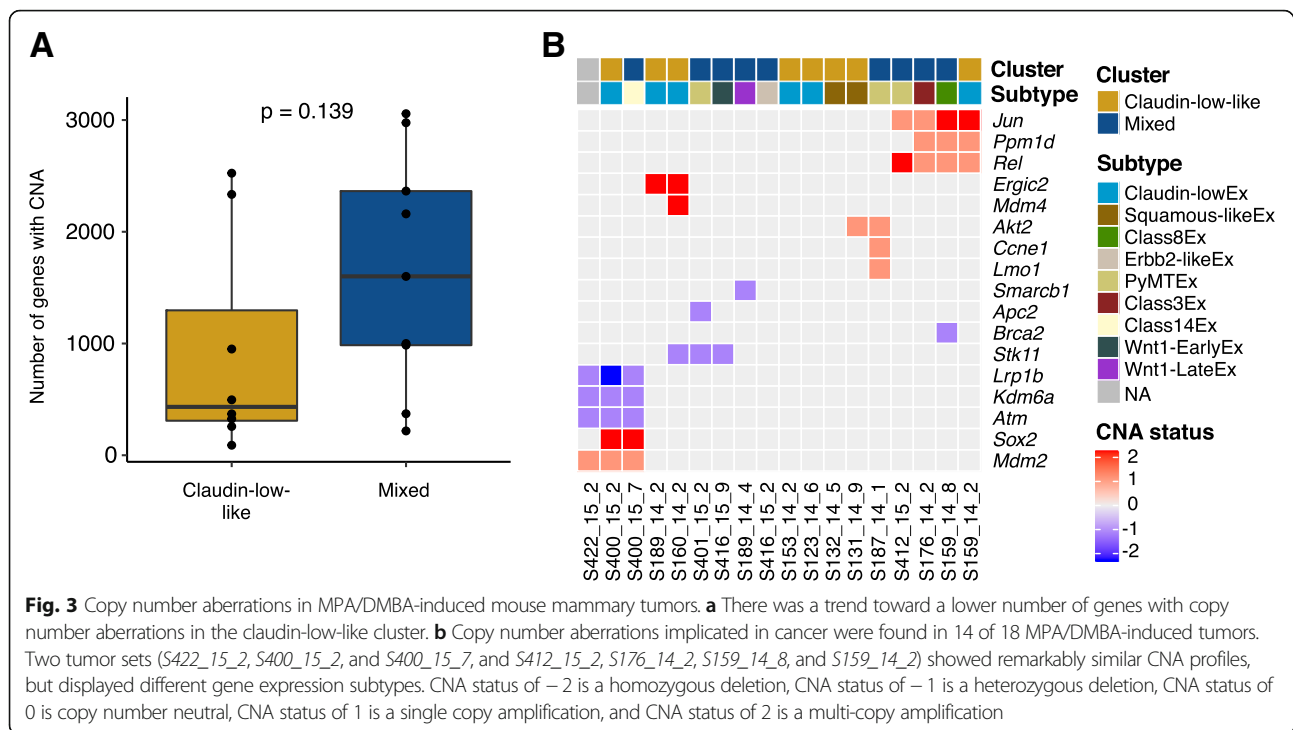
To determine CNAs in the MPA/DMBA-induced tumors with a potential oncogenic driver effect, we identified amplifications and deletions known to be associated with cancer [38] (Fig. 3b). We found that 14 of the 18 tumors carried potential driver CNAs (range 0 to 4, mean 2.6). Three of the four tumors not carrying potential driver CNAs were claudin-low-like. There was however no statistically significant difference in the number of potential driver CNAs between the clusters. Several genes had recurrent CNAs, but none occurred at a statistically significant different rate in one cluster versus the other.

Only two of the CNA events identified in MPA/DMBA-induced tumors occur at a notable rate in human breast cancer; *MDM4* is amplified in 25%, and *PPM1D* is amplified in 10% of human BC [6, 7].

We observed two sets of tumors carrying remarkably similar CNA profiles (Fig. 3b). None of the tumors in these two sets displayed the same murine subtype as any other tumor within the same set.

The human claudin-low breast cancer genome is characterized by a low mutational burden, frequent *TP53* mutations, and a low rate of CNA

Little has been published specifically describing the genomic characteristics of human claudin-low breast cancer. We therefore analyzed the 218 claudin-low tumors found in the METABRIC dataset, for which DNA



sequence data from 173 genes and whole genome copy number data is available [6, 7].

Across the 173 sequenced genes, claudin-low tumors carried a mean of 4.7 mutations per tumor, significantly lower than the mean of 7.3 mutations per tumor for all other tumors ($p < 0.001$, two-tailed Wilcoxon rank-sum test) (Fig. 4a). Claudin-low tumors share several characteristics with basal-like tumors and are often classified as such by the PAM50 assay [2, 6, 7]; however, basal-like tumors showed a significantly higher mutational burden than claudin-low tumors (mean 8.1 mutations per tumor, $p < 0.001$, two-tailed Wilcoxon rank-sum test).

There was a high degree of overlap between the genes most frequently mutated in claudin-low breast cancers and the genes most frequently mutated in all other breast cancers (Fig. 4b). Most of these genes carried mutations at similar rates between claudin-low and non-claudin-low tumors, albeit with a tendency toward a slightly lower rate in claudin-low tumors. There were however two notable differences in mutational frequency: a significantly higher rate of *TP53* mutations and a significantly lower rate of *PIK3CA* mutations in claudin-low tumors compared to other tumors. Similarly, basal-like tumors also carried a high frequency of *TP53* mutations and a low frequency of *PIK3CA* mutations [7, 44].

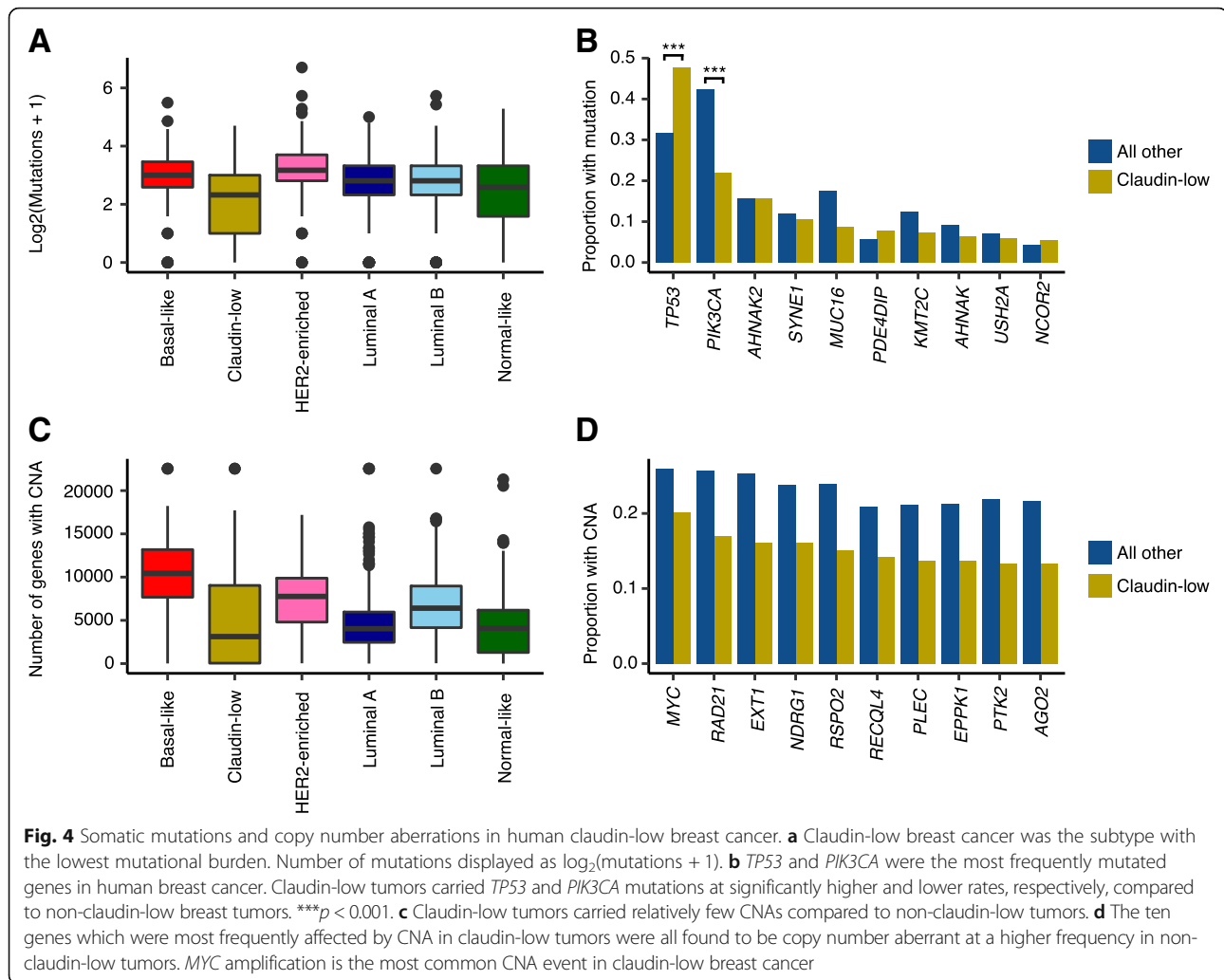
Human claudin-low breast tumors carried significantly fewer genes with copy number aberration (mean 4879) compared to all other tumors (mean 6247; $p < 0.001$, two-tailed Wilcoxon rank-sum test) (Fig. 4c). This

difference was also marked when comparing claudin-low tumors with basal-like tumors (mean 10,175 genes per tumor; $p < 0.001$, two-tailed Wilcoxon rank-sum test).

By gene, the most frequent copy number event in claudin-low breast cancer was *MYC* amplification, found in 20% of cases (Fig. 4d). In comparison, this event was found in 26% of all other breast tumors. The ten most frequently amplified genes in claudin-low breast cancer were all located at chromosomal position 8q24, a region also frequently amplified in basal-like breast cancers [6, 7].

Claudin-low-like MPA/DMBA-induced mammary tumors accurately reflect the gene expression characteristics of their human counterpart

We explored several established gene expression features of the claudin-low subtype and found that MPA/DMBA-induced claudin-low-like tumors accurately mirrored their human counterpart. Specifically, claudin-low-like tumors had low expression of genes involved in cell-cell adhesion, low expression of luminal genes, and high expression of genes related to EMT (Fig. 5a, Additional file 9). Claudin-low-like tumors also showed a markedly lower degree of differentiation compared to tumors in the mixed cluster. In particular, the claudin-low-like cluster expressed significantly higher and lower levels of *Cd44* and *Cd24a*, respectively, indicating a stem cell-like phenotype in these tumors [2, 60] (Additional file 10). There was no significant difference in the expression of proliferation-related genes between the two clusters. Vascular content-related genes were expressed at a significantly higher level in



claudin-low-like tumors compared to the tumors in the mixed cluster (Additional file 9), indicating a higher degree of neoangiogenesis in these tumors.

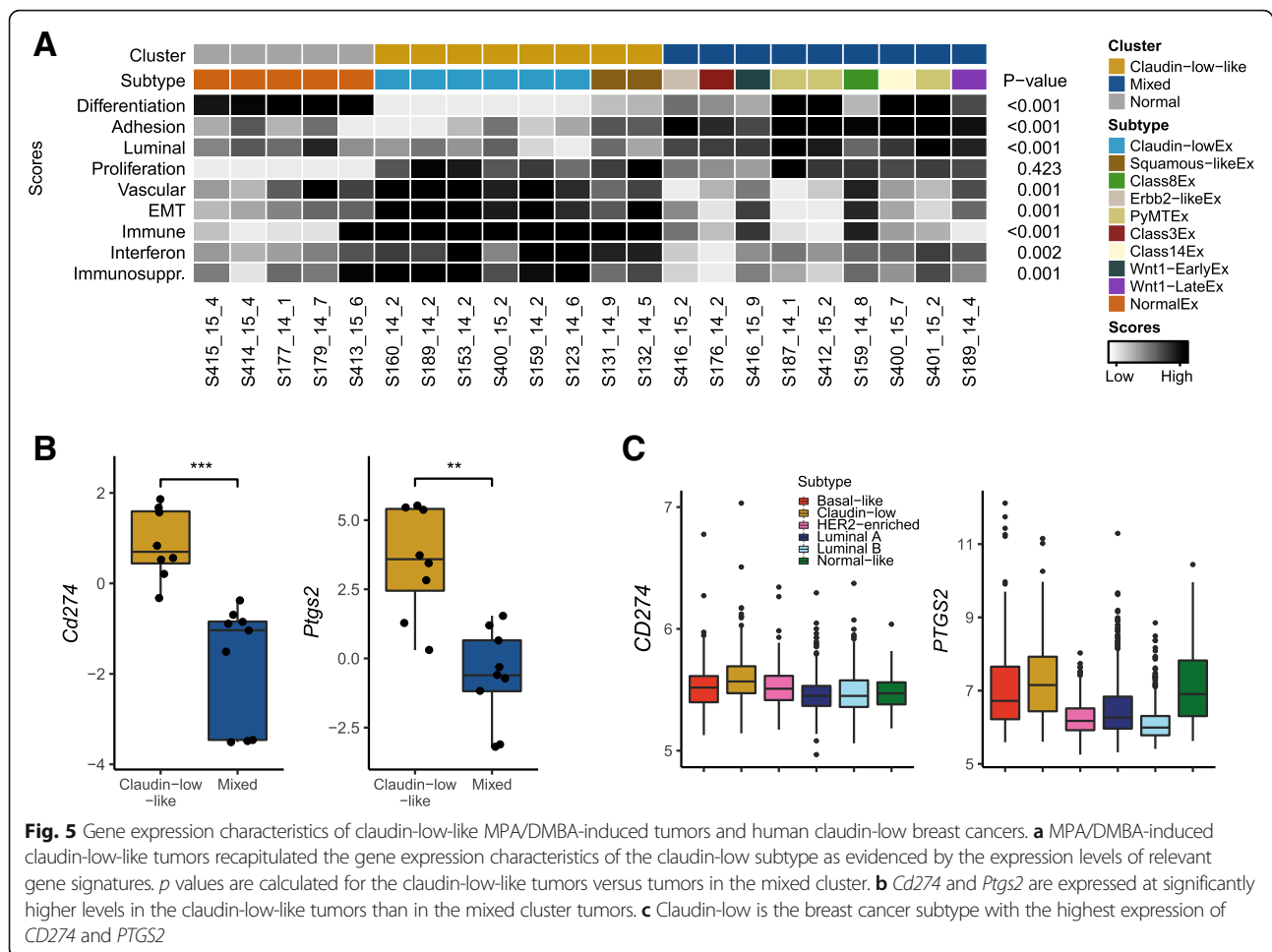
Immune cell admixture was significantly higher in the claudin-low-like tumors compared to tumors in the mixed cluster ($p < 0.001$, two-tailed Wilcoxon rank-sum test) and compared to normal mammary gland samples ($p = 0.006$). We also found higher expression of genes related to immunosuppression and interferons in the claudin-low-like cluster compared to both the mixed cluster and normal mammary gland samples. In combination, high immune cell infiltration and high expression of type 1 interferon-related and immunosuppressive genes are characteristics of tumors that may respond to immunotherapeutics [61, 62].

We identified a significantly elevated expression of two potentially actionable genes related to immunosuppression in the claudin-low-like tumors: the immune checkpoint encoding gene *Cd274* and the cyclooxygenase encoding gene *Ptgs2* (Fig. 5b). These features were also

characteristic of human claudin-low tumors in the METABRIC cohort [6, 7], which showed significantly higher expression levels of both *PTGS2* and *CD274* compared to non-claudin-low breast tumors ($p < 0.001$ for both, two-tailed Wilcoxon rank-sum test) and compared specifically to basal-like tumors ($p = 0.004$ and $p < 0.001$, respectively) (Fig. 5c). These characteristics may indicate a susceptibility to immune checkpoint inhibitors and cyclooxygenase inhibitors in human claudin-low breast cancer [63, 64].

Discussion

In this study, we have performed a comprehensive analysis of mutations, copy number aberrations, and gene expression characteristics of MPA/DMBA-induced mouse mammary tumors. We found marked intertumor heterogeneity and showed that half of the tumors displayed a claudin-low-like phenotype, in line with a previous report [11]. Our findings demonstrate that these tumors provide a transcriptomically accurate representation of human



claudin-low breast tumors, reflecting key features such as an EMT phenotype, high level of immune infiltration, and a low degree of differentiation.

MPA/DMBA-induced tumors carried a mutational burden multiple times that of human breast cancer, a high frequency of activating *Ras*-mutations, and a characteristic mutational spectrum. The specific genes carrying mutations varied widely between tumors; however, all tumors had a consistent mutational signature. This indicates that the dominant mutational process in these tumors is DMBA-induced mutagenesis, and not aberrations occurring after tumor initiation, as a result of, e.g., disrupted DNA repair. Copy number aberrations in MPA/DMBA-induced tumors have not previously been explored, and we show here that most tumors carry potential driver CNAs. However, while we noted several genomic trends, such as a higher rate of *Trp53* mutation and a lower burden of CNA in MPA/DMBA-induced claudin-low-like tumors, no individual genomic features accurately delineated the two gene expression-based tumor clusters. Further, several tumors carried similar sets of mutations and/or CNAs but displayed different

subtypes. This suggests that no specific genomic event determines tumor subtype and that other etiological models may be more appropriate, such as different cells-of-origin [65] or microenvironmental factors [66]. This finding concurs with recent reports showing that transgenic mouse mammary tumors display histological and transcriptomic phenotypes largely uncoupled from their underlying driver mutations [67–69]. One possible model for MPA/DMBA-induced tumorigenesis is therefore as follows: first, MPA induces a RANK-I-mediated mammary gland proliferation [10, 13]. DMBA then induces mutations in mammary cells in a pattern as elucidated by our mutation signature analysis, predominantly in TG and CA dinucleotides, stochastically distributed throughout the genome. The tumor is initiated when one or more driver mutations occur, for example, *Trp53* or *Ras*-mutation, with the tumor phenotype, however, determined by non-genomic factors. The biochemical mechanism of DMBA-induced mutagenesis has been described [14, 15], whereas no causal mechanism for DMBA-induced copy number aberration is known; it is therefore likely that CNAs arise after tumor initiation.

Previous genomic analyses which included human claudin-low breast tumors have either not included specific analyses of the subtype [6, 7], included few samples [3], or have been restricted to the triple-negative [70, 71] or metaplastic [72] subsets of claudin-low tumors. We show here that human claudin-low tumors are characterized by a low number of mutations and a low burden of CNAs. This finding is surprising, given the apparent inverse correlation between CNA and mutational burden in cancer [59], and indicates that the claudin-low subtype is relatively genomically stable compared to other breast cancers. We also find similarities in genomic characteristics between claudin-low tumors and basal-like tumors, in particular a high frequency of *TP53* mutations, a low frequency of *PIK3CA* mutations, and 8q24 amplifications as a common event. While the transcriptomic similarity between these two subtypes is established [2], these findings illustrate that there are also marked genomic similarities between claudin-low and basal breast cancer, albeit with a lower burden of genomic aberrations in claudin-low tumors.

Claudin-low tumors show high expression of immune-related genes and a high level of immune cell infiltration [2, 3, 73]. However, claudin-low tumors also express high levels of immunosuppressive genes. In MPA/DMBA-induced claudin-low-like tumors, we observed an elevated expression of two particularly notable genes involved in immunosuppression: *Ptgs2* (encoding COX-2) and *Cd274* (encoding PD-L1). This observation was consistent in human claudin-low breast cancer. COX-2 may be implicated in cancer development through several mechanisms: reducing apoptosis, increasing epithelial cell proliferation, promoting angiogenesis, and increasing invasiveness of tumor cells and immunosuppression [74–76]. COX-2 may also be involved in vasculogenic mimicry, a process in which epithelial tumor cells form vascular channel-like structures without participation of endothelial cells, allowing nutrients to reach tumor cells without the need for neoangiogenesis [77]. Vasculogenic mimicry has previously been shown to occur in claudin-low tumors [24]. COX-2 and PD-L1 are clinically actionable through the use of COX inhibitors [63] and checkpoint inhibitors [78], respectively. Further research into the potential use of checkpoint inhibitors and COX inhibitors in claudin-low breast cancer is warranted, with promising future avenues including combinatorial Treg depletion [73].

Conclusions

In summary, we have found that claudin-low-like MPA/DMBA-induced mouse mammary tumors are a transcriptomically accurate model for human claudin-low breast cancer. We did not find strong evidence that claudin-low-like MPA/DMBA-induced tumors are delineated by any specific genomic features; however, the relatively small

number of samples included in this study may have obscured possible associations. By analyzing publicly available data, we showed that human claudin-low breast cancer is a relatively genomically stable subtype. There is a high expression of genes related to immunosuppression in claudin-low breast cancers, a feature which is evident in claudin-low-like MPA/DMBA-induced tumors. Our observations suggest immunosuppression as a potential therapeutic target in claudin-low breast cancer and indicate MPA/DMBA-induced claudin-low-like tumors as an appropriate model for continued research.

Additional files

Additional file 1: Mouse characteristics and histopathological data. (XLSX 14 kb)

Additional file 2: Gene lists used for gene expression scores. (XLSX 11 kb)

Additional file 3: Subtype correlations for MPA/DMBA-induced tumors. (XLSX 17 kb)

Additional file 4: Mutations observed in MPA/DMBA-induced tumors. (XLSX 405 kb)

Additional file 5: Driver gene mutations in MPA/DMBA-induced tumors observed in the COSMIC database. (XLSX 37 kb)

Additional file 6: Comparative mutation rates in MPA/DMBA-induced tumors and human breast tumors in the TCGA cohort. (XLSX 27 kb)

Additional file 7: The mutational spectra and mutational signatures of MPA/DMBA-induced mammary tumors. **a** T>A transversions were the most frequent mutation type in MPA/DMBA-induced tumors, followed by C>A transversions. **b** Heatmap of mutational frequencies by trinucleotide context. There was an overrepresentation of T>N mutations in positions with a 3' guanine and C>N mutations in positions with a 3' adenine. **c** Histogram of C>A and T>A transversions by trinucleotide context in a representative tumor (*S159_14_8*). **d** Mutation signature 22 was the predominant mutational signature in the MPA/DMBA-induced tumors and was evident in all tumors in the cohort. (PDF 214 kb)

Additional file 8: Mutational signatures for all MPA/DMBA-induced tumors. (ZIP 142 kb)

Additional file 9: Gene expression scores by cluster for genes related to differentiation, adhesion, luminal features, proliferation, vascular content, EMT, immune features, interferon signaling and immunosuppression. Two-tailed Wilcoxon rank-sum test. ns = not significant, $p > 0.05$. * $p < 0.05$. ** $p < 0.01$. *** $p < 0.001$. (PDF 9 kb)

Additional file 10: Expression of *Cd24a* and *Cd44* by cluster in MPA/DMBA-induced tumors. Claudin-low-like tumors had a lower expression of *Cd24a* and a higher expression of *Cd44* compared to the mixed cluster of tumors ($p = 0.003$ and $p = 0.005$, respectively, two-tailed, Wilcoxon rank-sum test), indicating a stem cell-like phenotype in the claudin-low-like tumors. (PDF 5 kb)

Abbreviations

BC: Breast cancer; CNA: Copy number aberration; DMBA: 7,12-Dimethylbenzanthracene; EMT: Epithelial-mesenchymal transition; HE: Hematoxylin and eosin; MPA: Medroxyprogesterone acetate; PFA: Paraformaldehyde

Acknowledgements

We thank Phuong Vu, Eldri Undlien Due, and Tina Brinks for helping with the laboratory work; Prof. Rune Toftgård for providing the transgenic mouse lines; and the support staff at the Department of Comparative Medicine, Oslo University Hospital Norwegian Radium Hospital, for the help with the animal work. We are grateful to the members of the Department of Cancer

Genetics, Institute for Cancer Research, Oslo University Hospital, for insightful discussions, and in particular thank Tonje G. Lien for the statistical input.

Authors' contributions

CF, HB, JHN, and TS contributed to the conceptualization. CF, HB, RK, JHN, and TS contributed to the methodology. CF and HB contributed to the formal analysis. CF, HB, RK, JHN, and TS contributed to the investigation. JHN and TS contributed to the resources. CF and HB wrote the original draft of the manuscript. CF, HB, RK, JHN, and TS wrote, reviewed, and edited the manuscript. CF and HB contributed to the visualization. JHN and TS contributed to the supervision. TS contributed to the funding acquisition. All authors read and approved the final manuscript.

Funding

This work was supported by grants from the Norwegian Research Council (www.forskningradet.no/) (250459 to TS), South-Eastern Norway Regional Health Authority (www.helse-sorost.no/) (2012056 to TS), and the Medical Student Research Program at the University of Oslo (www.med.uio.no/) (to CF). The funders had no role in study design, data collection and analysis, decision to publish, or preparation of the manuscript.

Availability of data and materials

The datasets generated and/or analyzed during the current study are available in the European Nucleotide Archive, accession number PRJEB29718, and ArrayExpress, accession number E-MTAB-7507.

Ethics approval and consent to participate

The Norwegian Food Safety Authority approved all experiments in advance of their implementation (approval number 4385).

Consent for publication

Not applicable.

Competing interests

The authors declare that they have no competing interests.

Author details

¹Department of Cancer Genetics, Oslo University Hospital, Oslo, Norway. ²Department of Laboratory Medicine, Karolinska Institutet, Stockholm, Sweden. ³Centre for Cancer Biomarkers CCBIO, University of Bergen, Bergen, Norway. ⁴Institute for Clinical Medicine, University of Oslo, Oslo, Norway.

Received: 5 March 2019 Accepted: 17 July 2019

Published online: 31 July 2019

References

- Herschkwitz JI, Simin K, Weigman VJ, Mikaelian I, Usary J, Hu Z, et al. Identification of conserved gene expression features between murine mammary carcinoma models and human breast tumors. *Genome Biol.* 2007;8(5):R76.
- Prat A, Parker JS, Karginova O, Fan C, Livasy C, Herschkowitz JI, et al. Phenotypic and molecular characterization of the claudin-low intrinsic subtype of breast cancer. *Breast Cancer Res.* 2010;12(5):R68.
- Sabatier R, Finetti P, Guille A, Adelaide J, Chaffanet M, Viens P, et al. Claudin-low breast cancers: clinical, pathological, molecular and prognostic characterization. *Mol Cancer.* 2014;13(1):228.
- Prat A, Perou CM. Deconstructing the molecular portraits of breast cancer. *Mol Oncol.* 2011;5(1):5–23.
- Dias K, Dvorkin-Gheva A, Hallett RM, Wu Y, Hassell J, Pond GR, et al. Claudin-low breast cancer; clinical & pathological characteristics. *PLoS One.* 2017; 12(1):e0168669.
- Curtis C, Shah SP, Chin S-F, Turashvili G, Rueda OM, Dunning MJ, et al. The genomic and transcriptomic architecture of 2,000 breast tumours reveals novel subgroups. *Nature.* 2012;486(7403):346.
- Pereira B, Chin S-F, Rueda OM, Vollan H-KM, Provenzano E, Bardwell HA, et al. The somatic mutation profiles of 2,433 breast cancers refine their genomic and transcriptomic landscapes. *Nat Commun.* 2016;7:11479.
- Hennessy BT, Gonzalez-Angulo A-M, Stemke-Hale K, Gilcrease MZ, Krishnamurthy S, Lee J-S, et al. Characterization of a naturally occurring breast cancer subset enriched in epithelial-to-mesenchymal transition and stem cell characteristics. *Cancer Res.* 2009;69(10):4116–24.
- Prat A, Adamo B, Cheang MCU, Anders CK, Carey LA, Perou CM. Molecular characterization of basal-like and non-basal-like triple-negative breast cancer. *Oncologist.* 2013;18(2):123–33.
- Aldez CM, Liao QY, LaBate M, Johnston DA. Medroxyprogesterone acetate accelerates the development and increases the incidence of mouse mammary tumors induced by dimethylbenzanthracene. *Carcinogenesis.* 1996;17(9):2069–72.
- Pfefferle AD, Herschkowitz JI, Usary J, Harrell J, Spike BT, Adams JR, et al. Transcriptomic classification of genetically engineered mouse models of breast cancer identifies human subtype counterparts. *Genome Biol.* 2013; 14(11):R125.
- Yin Y, Bai R, Russell RG, Beildeck ME, Xie Z, Kopelovich L, et al. Characterization of medroxyprogesterone and DMBA-induced multilineage mammary tumors by gene expression profiling. *Mol Carcinog.* 2005;44(1): 42–50.
- Gonzalez-Suarez E, Jacob AP, Jones J, Miller R, Roudier-Meyer MP, Erwert R, et al. RANK ligand mediates progesterin-induced mammary epithelial proliferation and carcinogenesis. *Nature.* 2010;468(7320):103.
- Baird WM, Hooven LA, Mahadevan B. Carcinogenic polycyclic aromatic hydrocarbon-DNA adducts and mechanism of action. *Environ Mol Mutagen.* 2005;45(2–3):106–14.
- Frenkel K. 7,12-dimethylbenz[a]anthracene induces oxidative DNA modification in vivo. *Free Radic Biol Med.* 1995;19(3):373–80.
- Dean JH, Ward EC, Murray MJ, Lauer LD, House RV. Mechanisms of dimethylbenzanthracene-induced immunotoxicity. *Clin Physiol Biochem.* 1985;3(2–3):98–110.
- Miyata M, Furukawa M, Takahashi K, Gonzalez FJ, Yamazoe Y. Mechanism of 7, 12-dimethylbenz[a]anthracene-induced immunotoxicity: role of metabolic activation at the target organ. *Jpn J Pharmacol.* 2001;86(3):302–9.
- Trichopoulos D, Adami H, Ekbohm A, Hsieh C, Lagiou P. Early life events and conditions and breast cancer risk: from epidemiology to etiology. *Int J Cancer.* 2008;122(3):481–5.
- Snippert HJ, Van Der Flier LG, Sato T, Van Es JH, Van Den Born M, Kroon-Veenboer C, et al. Intestinal crypt homeostasis results from neutral competition between symmetrically dividing Lgr5 stem cells. *Cell.* 2010; 143(1):134–44.
- Norum JH, Bergström Å, Andersson AB, Kuiper RV, Hoelzl MA, Sørli T, et al. A conditional transgenic mouse line for targeted expression of the stem cell marker LGR5. *Dev Biol.* 2015;404(2):35–48.
- Team RC. Computing RF, for S. R. A language and environment for statistical computing. Vienna: R Foundation for Statistical Computing; 2017.
- Liu Y, Hayes DN, Nobel A, Marron JS. Statistical significance of clustering for high-dimension, low-sample size data. *J Am Stat Assoc.* 2008;103(483):1281–93.
- Yoshihara K, Shahmoradgoli M, Martínez E, Vegesna R, Kim H, Torres-Garcia W, et al. Inferring tumour purity and stromal and immune cell admixture from expression data. *Nat Commun.* 2013;4:2612.
- Chuck Harrell J, Pfefferle AD, Zalles N, Prat A, Fan C, Khramtsov A, et al. Endothelial-like properties of claudin-low breast cancer cells promote tumor vascular permeability and metastasis. *Clin Exp Metastasis.* 2014;31:33–45.
- Kardos J, Chai S, Mose LE, Selitsky SR, Krishnan B, Saito R, et al. Claudin-low bladder tumors are immune infiltrated and actively immune suppressed. *JCI insight.* 2016;1(3):e85902.
- TO N, Parker JS, Leung S, Voduc D, Ebbert M, Vickery T, et al. A comparison of PAM50 intrinsic subtyping with immunohistochemistry and clinical prognostic factors in tamoxifen-treated estrogen receptor-positive breast cancer. *Clin Cancer Res.* 2010;16(21):5222–32.
- Subramanian A, Tamayo P, Mootha VK, Mukherjee S, Ebert BL, Gillette MA, et al. Gene set enrichment analysis: a knowledge-based approach for interpreting genome-wide expression profiles. *Proc Natl Acad Sci.* 2005; 102(43):15545–50.
- Andrews S. FastQC: a quality control tool for high throughput sequence data. 2010. Available from: <http://www.bioinformatics.babraham.ac.uk/projects/fastqc>
- Martin M. Cutadapt removes adapter sequences from high-throughput sequencing reads. *EMBnet J.* 2011;17(1):10–2.
- Joshi NAFJN. Sickle: a sliding-window, adaptive, quality-based tool for FastQ files; 2011.
- Li H. Aligning sequence reads, clone sequences and assembly contigs with BWA-MEM. *arXiv:13033997*; 2013.
- Van der Auwera GA, Carneiro MO, Hartl C, Poplin R, del Angel G, Levy-Moonshine A, et al. From FastQ data to high-confidence variant calls: the

- genome analysis toolkit best practices pipeline. In: Current protocols in bioinformatics: Wiley; 2013. <https://doi.org/10.1002/0471250953.bi1110s43>.
33. McKenna A, Hanna M, Banks E, Sivachenko A, Cibulskis K, Kernysky A, et al. The Genome Analysis Toolkit: a MapReduce framework for analyzing next-generation DNA sequencing data. *Genome Res.* 2010;20(9):1297–303.
 34. DePristo MA, Banks E, Poplin R, Garimella KV, Maguire JR, Hartl C, et al. A framework for variation discovery and genotyping using next-generation DNA sequencing data. *Nat Genet.* 2011;43(5):491–8.
 35. Wong K, Bumpstead S, Van Der Weyden L, Reinholdt LG, Wilming LG, Adams DJ, et al. Sequencing and characterization of the FVB/NJ mouse genome. *Genome Biol.* 2012;13(8):1–12.
 36. Cingolani P, Platts A, Wang LL, Coon M, Nguyen T, Wang L, et al. A program for annotating and predicting the effects of single nucleotide polymorphisms, SnpEff. *Fly (Austin).* 2012;6(2):80–92.
 37. Cingolani P, Patel VM, Coon M, Nguyen T, Land SJ, Ruden DM, et al. Using *Drosophila melanogaster* as a model for genotoxic chemical mutational studies with a new program. *SnpSift Front Genet.* 2012;3:35.
 38. Forbes SA, Beare D, Boutselakis H, Bamford S, Bindal N, Tate J, et al. COSMIC: somatic cancer genetics at high-resolution. *Nucleic Acids Res.* 2016;45(D1):D777–83.
 39. Sievers F, Wilm A, Dineen D, Gibson TJ, Karplus K, Li W, et al. Fast, scalable generation of high-quality protein multiple sequence alignments using Clustal Omega. *Mol Syst Biol.* 2014;7(1):539.
 40. The UniProt Consortium. UniProt: the universal protein knowledgebase. *Nucleic Acids Res.* 2017;45(D1):D158–69.
 41. Rosenthal R, McGranahan N, Herrero J, Taylor BS, Swanton C. deconstructSigs: delineating mutational processes in single tumors distinguishes DNA repair deficiencies and patterns of carcinoma evolution. *Genome Biol.* 2016;17(1):1.
 42. Alexandrov LB, Nik-Zainal S, Wedge DC, Aparicio SA, Behjati S, Biankin AV, et al. Signatures of mutational processes in human cancer. *Nature.* 2013;500(7463):415–21.
 43. D'Aurizio R, Pippucci T, Tattini L, Giusti B, Pellegrini M, Magi A. Enhanced copy number variants detection from whole-exome sequencing data using EXCAVATOR2. *Nucleic Acids Res.* 2016;44(20):e154.
 44. The Cancer Genome Atlas Network. Comprehensive molecular portraits of human breast tumours. *Nature.* 2012;490(7418):61.
 45. Gao J, Aksoy BA, Dogrusoz U, Dresdner G, Gross B, Sumer SO, et al. Integrative analysis of complex cancer genomics and clinical profiles using the cBioPortal. *Sci Signal.* 2013;6(269):pl1.
 46. Cerami E, Gao J, Dogrusoz U, Gross BE, Sumer SO, Aksoy BA, et al. The cBio cancer genomics portal: an open platform for exploring multidimensional cancer genomics data. *ACR; 2012.* <https://doi.org/10.1158/2159-8290.CD-12-0095>.
 47. Gu Z, Eils R, Schlesner M. Complex heatmaps reveal patterns and correlations in multidimensional genomic data. *Bioinformatics.* 2016;32(18):2847–9.
 48. Wickham H. *ggplot2*. New York: Springer New York; 2009.
 49. Lawrence MS, Stojanov P, Polak P, Kryukov GV, Cibulskis K, Sivachenko A, et al. Mutational heterogeneity in cancer and the search for new cancer-associated genes. *Nature.* 2013;499(7457):214–8.
 50. McCreery MQ, Halliwill KD, Chin D, Delrosario R, Hirst G, Vuong P, et al. Evolution of metastasis revealed by mutational landscapes of chemically induced skin cancers. *Nat Med.* 2015;21(12):1514.
 51. Westcott PMK, Halliwill KD, To MD, Rashid M, Rust AG, Keane TM, et al. The mutational landscapes of genetic and chemical models of Kras-driven lung cancer. *Nature.* 2015;517(7535):489–92.
 52. Nassar D, Latil M, Boeckx B, Lambrechts D, Blanpain C. Genomic landscape of carcinogen-induced and genetically induced mouse skin squamous cell carcinoma. *Nat Med.* 2015;21(8):946.
 53. Francis JC, Melchor L, Campbell J, Kendrick H, Wei W, Armisen-Garrido J, et al. Whole-exome DNA sequence analysis of Brca2-and Trp53-deficient mouse mammary gland tumours. *J Pathol.* 2015;236(2):186–200.
 54. Pfefferle AD, Agrawal YN, Koboldt DC, Kanchi KL, Herschkowitz JI, Mardis ER, et al. Genomic profiling of murine mammary tumors identifies potential personalized drug targets for p53-deficient mammary cancers. *Dis Model Mech.* 2016;9(7):749–57.
 55. Liu H, Murphy CJ, Karreth FA, Emdal KB, White FM, Elemento O, et al. Identifying and targeting sporadic oncogenic genetic aberrations in mouse models of triple-negative breast cancer. *Cancer Discov.* 2018;8(3):354–69.
 56. McFadden DG, Politi K, Bhutkar A, Chen FK, Song X, Pirun M, et al. Mutational landscape of EGFR-, MYC-, and Kras-driven genetically engineered mouse models of lung adenocarcinoma. *Proc Natl Acad Sci.* 2016;113(42):E6409–17.
 57. McFadden DG, Papagiannakopoulos T, Taylor-Weiner A, Stewart C, Carter SL, Cibulskis K, et al. Genetic and clonal dissection of murine small cell lung carcinoma progression by genome sequencing. *Cell.* 2014;156(6):1298–311.
 58. Abba MC, Zhong Y, Lee J, Kil H, Lu Y, Takata Y, Simper MS, Gaddis S, Shen J, Aldaz CM. DMBA induced mouse mammary tumors display high incidence of activating Pik3caH1047 and loss of function Pten mutations. *Oncotarget.* 2016;7(39):64289.
 59. Ciriello G, Miller ML, Aksoy BA, Senbabaoglu Y, Schultz N, Sander C. Emerging landscape of oncogenic signatures across human cancers. *Nat Genet.* 2013;45(10):1127–33.
 60. Visvader JE, Stingl J. Mammary stem cells and the differentiation hierarchy: current status and perspectives. *Genes Dev.* 2014;28(11):1143–58.
 61. Hegde PS, Karanikas V, Evers S. The where, the when, and the how of immune monitoring for cancer immunotherapies in the era of checkpoint inhibition. *Clin Cancer Res.* 2016;22(8):1865–74.
 62. Jamieson NB, Maker AV. Gene-expression profiling to predict responsiveness to immunotherapy. *Nat Publ Gr.* 2016;24(3):134–40.
 63. Zelenay S, Van Der Veen AG, Böttcher JP, Snelgrove KJ, Rogers N, Acton SE, et al. Cyclooxygenase-dependent tumor growth through evasion of immunity. *Cell.* 2015;162(6):1257–70.
 64. Chokr N, Chokr S. Immune checkpoint inhibitors in triple negative breast cancer: what is the evidence? *J Neoplasm.* 2018;3(2):6.
 65. Prat A, Perou CM. Mammary development meets cancer genomics. *Nat Med.* 2009;15(8):842.
 66. Hanahan D, Coussens LM. Accessories to the crime: functions of cells recruited to the tumor microenvironment. *Cancer Cell.* 2012;21(3):309–22.
 67. Hollern DP, Swiatnicki MR, Andrechek ER. Histological subtypes of mouse mammary tumors reveal conserved relationships to human cancers. *PLoS Genet.* 2018;14(1):e1007135.
 68. Rennhack J, Swiatnicki M, Zhang Y, Li C, Bylett E, Ross C, Szczepanek K, Hanrahan W, Jayatissa M, Hunter K, Andrechek E. Integrated sequence and gene expression analysis of mouse models of breast cancer reveals critical events with human parallels. *bioRxiv.* 2018;375154. <https://www.biorxiv.org/content/10.1101/375154v1.full>.
 69. Hollern DP, Andrechek ER. A genomic analysis of mouse models of breast cancer reveals molecular features of mouse models and relationships to human breast cancer. *Breast Cancer Res.* 2014;16(3):R59.
 70. Morel A-P, Ginstier C, Pommier RM, Cabaud O, Ruiz E, Wicinski J, et al. A stemness-related ZEB1–MSRB3 axis governs cellular pliancy and breast cancer genome stability. *Nat Med.* 2017;23(5):568.
 71. Burstein MD, Tsimelzon A, Poage GM, Covington KR, Contreras A, Fuqua SAW, et al. Comprehensive genomic analysis identifies novel subtypes and targets of triple-negative breast cancer. *Clin Cancer Res.* 2015;21(7):1688–98.
 72. Weigelt B, Ng CKY, Shen R, Popova T, Schizas M, Natrajan R, et al. Metastatic breast carcinomas display genomic and transcriptomic heterogeneity. *Mod Pathol.* 2015;28(3):340.
 73. Taylor NA, Vick SC, Iglesia MD, Brickey WJ, Midkiff BR, McKinnon KP, et al. Treg depletion potentiates checkpoint inhibition in claudin-low breast cancer. *J Clin Invest.* 2017;127(9):3472–83.
 74. Zarghi A, Arfaei S. Selective COX-2 inhibitors: a review of their structure-activity relationships. *Iran J Pharm Res IJPR.* 2011;10(4):655–83.
 75. Dannenberg AJ, DuBois RN. COX-2: a new target for cancer prevention and treatment. *Karger; 2003.* p. 291. <https://scholar.google.com/scholar?cluster=4132316902324774708>.
 76. Tsujii M, DuBois RN. Alterations in cellular adhesion and apoptosis in epithelial cells overexpressing prostaglandin endoperoxide synthase 2. *Cell.* 1995;83(3):493–501.
 77. Basu GD, Liang WS, Stephan DA, Wegener LT, Conley CR, Pockaj BA, et al. A novel role for cyclooxygenase-2 in regulating vascular channel formation by human breast cancer cells. *Breast Cancer Res.* 2006;8(6):R69.
 78. Yan X, Zhang S, Deng Y, Wang P, Hou Q, Xu H. Prognostic factors for checkpoint inhibitor based immunotherapy: an update with new evidences. *Front Pharmacol.* 2018;9:1050.

Publisher's Note

Springer Nature remains neutral with regard to jurisdictional claims in published maps and institutional affiliations.